Kirk-Othmer Encyclopedia of Chemical Technology.

GLASSY METALS

Materials can be classified in several ways, one of which is by atomic structure, ie, whether the material is periodic (crystalline) or nonperiodic (amorphous) in space. Most metals, minerals, and ceramics are crystalline having the atoms arranged in periodic form and having translational symmetry. The bulk of materials that are nonperiodic is composed of various oxide glasses but also includes amorphous or glassy metals. These metallic glasses do not occur naturally but are produced by various techniques, the oldest of which is by cooling molten metals so rapidly that the atoms do not get to form regular crystalline structures. The atoms are frozen in random or nonrepeating atomic patterns similar to those found in organic glasses (see Glass). By metallic it is meant that the amorphous material is composed primarily, but not necessarily exclusively, of metallic elements that exhibit the properties of metals such as electrical or magnetic behavior.

The first synthesis of a metallic glass drawing wide attention among material scientists occurred in 1960 (1). A liquid gold–silicon alloy, when rapidly quenched to the temperature of liquid nitrogen, was reported to form a glass. Numerous metallic alloys have been amorphized using this melt-quenching technique. These have a wide variety of elements and compositions (2, 3). A drawback of the early techniques is that one or more of the dimensions had to be thin, often as thin as 15 μm, making it unlikely that metallic glasses would be used for structural applications. Primarily through modification of the chemistries, glasses have been produced that can truly be considered bulk, even exceeding 1 cm in all dimensions (4). Warm extrusion and consolidation of metallic glass powders (5) produce blocks of glassy metals that can later be machined into components. Besides rapid solidification into thin ribbons or flakes, there exists a wide range of techniques to produce metallic glass. Methods available include chemical means (6), mechanical alloying (7, 8) vaporization (9), and solid-state reactions (10).

Interest is maintained in these materials because of the combination of mechanical, corrosion, electric, and magnetic properties. However, it is their ferromagnetic properties that lead to the principal application of glassy metals. The soft magnetic properties and remarkably low coercivity offer tremendous opportunities for this application (see Magnetic materials, bulk; Magnetic materials, thin film).

A limitation of metallic glass is that it exists in metastable form, which means that it tends to crystallize if heated with sufficient thermal energy to allow the kinetics of crystallization, ie, both nucleation and growth, to occur. If glassy metal alloys were all intrinsically unstable, however, they would be much less promising as an engineering material. Understanding the solid-state structure, the unusual mechanical properties, the liquid-like electrical properties, and the ferromagnetic properties of metallic glasses has been the focus of research and development efforts since the late 1950s.

1. Structure of Metallic Glass

An understanding of glassy metal alloys begins with an understanding of conventionally processed metal alloys. Macroscopically crystalline metals and metallic glasses look and feel the same. Atomistically, under normal conditions, metals and metal alloys are crystalline, ie, the atoms are arranged in a periodically repeated

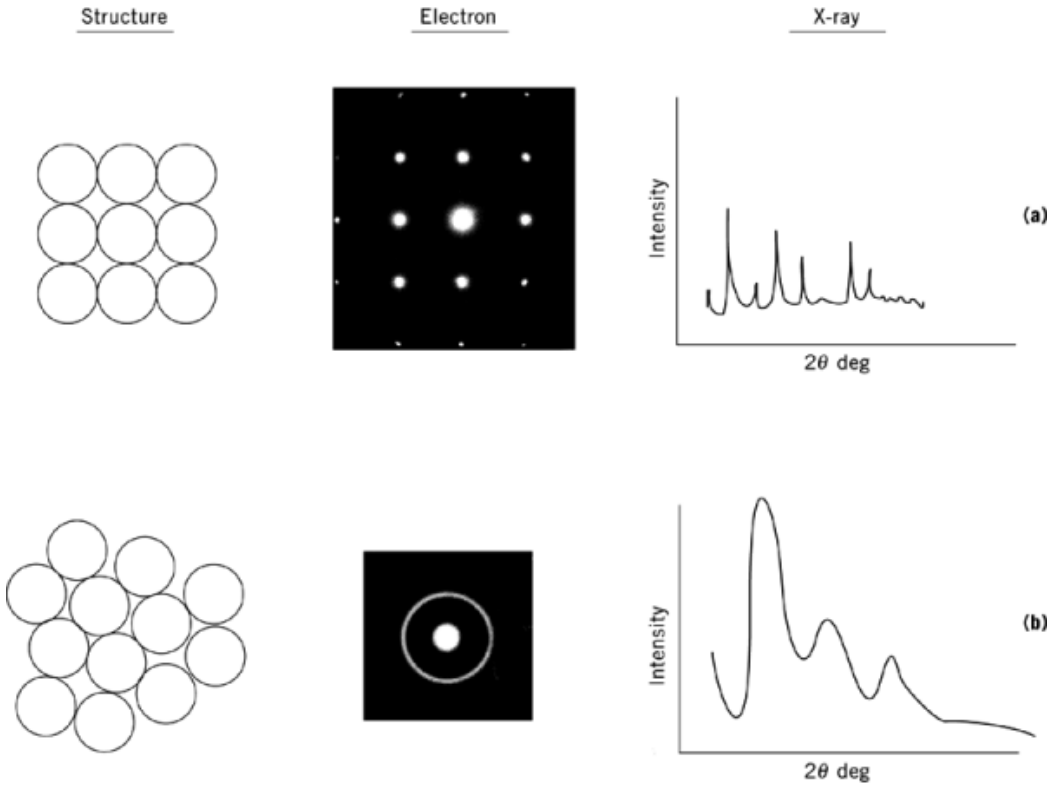

Fig. 1. Structures of (○) atoms and corresponding electron and x-ray diffraction patterns for (**a**) a periodic arrangement exhibiting translational symmetry where the bright dots and sharp peaks prove the periodic symmetry of the atoms by satisfying the Bragg condition, and (**b**) in a metallic glass where the atoms are nonperiodic and have no translational symmetry. The result of this structure is that the diffraction is diffuse.

three-dimensional pattern (Fig. 1**a**). In amorphous materials the atoms are arranged more or less randomly (Fig. 1**b**), although there may be regions of local order owing to constraints imposed by the close packing of atoms as the melt solidifies. This order, however, is not repeated over large distances in the solid, and in general, these regions are very localized and widely spaced. Various experimental diffraction techniques are customarily used to determine the structure of metals. These include x-ray, neutron, and electron diffraction techniques (see Fig.1). X-ray diffraction is the most popular and historically most important method in the structural analysis of metallic glasses (see X-ray technology).

Diffraction occurs when the Bragg equation is satisfied, resulting in well-known diffraction patterns having sharp intensity peaks. In amorphous materials, the unordered assemblages of atoms interact with radiation in such a way as to produce a dispersed, nondistinctive pattern. Because the range of the core electrons distributed around the nucleus is nearly the same as the x-ray wavelength, the phase of the scattered x-rays depends on the position of the electron corresponding to the origin of scattering in the atoms. Thus the atomic scattering factor of x-rays drastically decreases with an increase in the scattering angle. In contrast, the wavelength of the thermal neutrons used in general diffraction experiments is considerably larger than the size of the nucleus ($\simeq 10^{-12}$ cm); ie, the scattering amplitude is independent of the scattering angle. Whereas electron diffraction as recorded on photographic film has relatively poor quantitative intensity accuracy, this can be improved by employing digitally recorded images in modern electron microscopes (see Microscopy).

Advantages of electron diffraction are that the difference in angular dependence is smaller than that for x-ray diffraction. This is important in systems that contain both light and heavy elements, in that the effect of the light elements plays a significant role in scattering intensity in the low scattering angle regions.

The description of the atomic distribution in noncrystalline materials employs a distribution function, $g(r)$, which corresponds to the probability of finding another atom at a distance r from the origin atom taken as the point $r = 0$. In a system having an average number density $\rho = N/V$, the probability of finding another atom at a distance r from an origin atom corresponds to $\rho_0 g(r)$. Whereas the information given by $g(r)$, which is called the pair distribution function, is only one-dimensional, it is quantitative information on the noncrystalline systems and as such is one of the most important pieces of information in the study of noncrystalline materials. The interatomic distances cannot be smaller than the atomic core diameters, so $g(r)_{r \longrightarrow 0} = 0$. Because the correlation of atomic positions decreases as $r \longrightarrow \infty$, $g(r)_{r \longrightarrow \infty} = 1$. The function $4\pi^2 \rho g_o(r)$, the radial distribution function (RDF), may also be used in the discussion of noncrystalline systems. This function corresponds to the number of atoms in the spherical shell between r and $r + dr$.

Because glasses do not possess a crystal structure, atomic positions can only be described on a statistical basis. Assessment of the amorphous structure involves the determination of the radial (or pair) distribution structure and the use of modeling (2, 11). Complementary experiments, eg, Mössbauer spectroscopy or nuclear magnetic resonance (12), are useful because the radial distribution function does not provide a total picture of the amorphous structure. The models that are compared with experimental results include the dense random packing (DRP) model (13); an extension of the DRP model obtained by introducing chemical ordering (2, 11); and a model based on prism packing of small identifiable units of a stable crystalline structure (14). The models become increasingly sophisticated depending on the experimental detail considered.

The DRP model can be appreciated by considering the packing and kneading of hard balls in a rubber bag. Subsequent analysis of the resulting structure reveals basic structural polyhedra units. Tetrahedral and octahedral units make up the majority of the structure, the ratio of frequency of various polyhedra in the structure, however, has not been agreed on. The model does agree with computed RDF for some metallic glasses but for metal–metalloid systems the smaller atom is sometimes not included. An improvement of this model results when the condition of hard spheres is removed. Use of soft atoms has led to better agreement. Many approximations to the model remain, however, leading to other difficulties.

It is generally accepted that pure metals cannot be quenched from the liquid state into a metallic glass using the cooling rates available as of this writing. Many alloys cannot be turned into glasses either. Alloy phase theory is not developed sufficiently to predict the composition of a metallic alloy that can be quenched into a glass, but there are experimental guidelines (2, 15). Systems having a deep eutectic lying in the glass-forming composition region and systems composed of elements undergoing strong interactions, ie, negative free energy of mixing, often form glasses. Many glasses contain both a strongly metallic element including Fe, Co, Ni, Pd, Pt, Cu, and a nonmetallic element or metalloid eg, B^{3+} forms Fe–B; C, Si, or Ge of valence 4, forms Au–Si for example; or P of valence 5, forms Cu–P. Binary metal alloys include Cu–Zr, Nb–Ni, Ta–Ni, Y–Cu, and Ti–Ni (2). Ternary alloys that can produce glass may include two metals and one metalloid such as Pd–Ni–P, or one metal and two metalloids, such as Fe–P–B. For ternaries, the metallic elements make up to 70–85 atomic % of the material. The remaining atomic % is metalloid (15). A simple list of glass-forming systems includes (*1*) intertransition metals, (*2*) transition-metal—metalloid (semimetal), (*3*) systems based on alkaline-earths, and (*4*) the actinide–transition-metal system (8). Examples of the various categories of metallic glasses are given in Table 1.

A family of glasses discovered in 1988 (16–19) is based on aluminum, a rare-earth (RE) element, and a transition metal (TM) (see Aluminum and aluminum alloys). Aluminum contents may be as high as 90 atomic %. The empirical rules of predicting metallic glass compositions became even more difficult after this discovery because of the unusual glass formability in these Al-based metallic glasses. For conventional amorphous alloys, the glass-formation range usually coincides with a deep eutectic region where the liquid is stable to a lower temperature than in other regions of the phase diagram. In principle, the degree of supercooling required to

Table 1. Metallic Glasses

Alloy	Useful properties/applications
$Fe_{78}B_{13}Si_9$	Metglas 2605S2,[a] good magnetic properties
$Fe_{80}B_{20}$	Metglas 2605[a]
$Pd_{80}Si_{20}$	easy to form glass, thick samples produced
$Pt_{60}Ni_{15}P_{25}$	
$Cu_{84.3}P_{15.7}$ eutectic	brazing foil
$Al_{85}Ni_5Fe_2Gd_8$	high strength low density thick ribbons
$Mg_{80}Cu_{15}Sn_5$	low density cast 4-mm dia rods
$Co_{83}Gd_{17}$	sputtered sample can support magnetic bubbles
$Mo_{64}Re_{16}P_{10}B_{10}$	superconducting below 8.7 K
$W_{60}Ir_{20}B_{20}$	crystallization temperature above 1200 K
$Zr_{41.2}Ti_{13.8}Cu_{12.5}Ni_{10}Be_{22.5}$	14-mm rod produced

[a]Produced by AlliedSignal.

form a glassy state is reduced in the eutectic region, and crystallization can be suppressed more easily, thus allowing the formation of metallic glass. A significant difference from the usual glass-forming systems is that liquidus temperatures of the Al–RE binary alloys increase rapidly as minority RE is added to Al; yet the glass formation in $Al_{100--x}RE_x$ has been demonstrated for $x = 8 - 16$ for Gd, $x = 1 - 10$ for La or Ce, $x = 9 - 13$ for Y, and $x = 8 - 16$ for Sm (see Lanthanides). This was totally unexpected (18, 19).

2. Formability

A molten metal alloy would normally be expected to crystallize into one or several phases. To form an amorphous, ie, glassy metal alloy from the liquid state means that the crystallization step must be avoided during solidification. This can be understood by considering a time–temperature–transformation (TTT) diagram (Fig. 2). Nucleating phases require an incubation time to assemble atoms through a statistical process into the correct crystal structure which is capable of surmounting an activation barrier ΔG^* (Fig. 3). Incubation times can vary from fractions of a second to many seconds. The shape of the TTT curve is in the form of a C because of competing phenomena. As temperature is lowered, the free energy available to nucleate and grow a crystalline phase increases but the kinetic ability to do so through atomic diffusion decreases, resulting in a nose at T' (see Crystallization; Zone refining). The glass-forming ability of a material is determined by the kinetics of this process followed by the initial stages of crystal growth (20). If the liquid alloy is cooled from above the melting temperature to a temperature below the nose of the TTT curve at T' within a time less than the time where crystallization begins (eg, Fig. 2, part A), the alloy's liquid-like structure becomes frozen in when the temperature drops below the glass-forming temperature, T_g, whereby an amorphous solid is obtained. Once the alloy is below T_g, diffusion processes are such that growth of a crystalline embryo (Fig. 3) is essentially halted, and the liquid structure is preserved.

A reduced glass temperature can be defined as $T_{rg} = T_g/T_l$ which represents a measure of glass-forming ability. The higher the T_g and the lower the liquidus temperature, T_l, the easier it is to supercool the metal melt to a glassy state. Conventional theory predicts $T_{rg} = 0.65 - 0.7$ for good glass formers, eg, $T_{rg} \simeq 0.63$ for $Pd_{77}Cu_6Si_{17}$, and $T_{rg} \simeq 0.67$ for $Pd_{40}Ni_{40}P_{20}$, where a quenching rate as low as 100–1000 K/s is sufficient to produce the glassy state (21–23). However, substantially smaller T_{rg} values were observed for Al–Ni–Fe–Gd metallic glasses. For example T_{rg} for $Al_{85}Ni_5Fe_2Gd_8$ is about 0.44, which is close to the lowest limit of T_{rg} in glass-forming metallic systems previously observed. In chalcogenide alloys such as Ge_xSe_{100--x}, easy glass formation by air or water quenching has been observed in the region where the system exhibits only low (0.4–0.5) T_{rg} (24). However, high (10^9–10^{10} K/s) cooling rates are generally required to melt-quench metallic

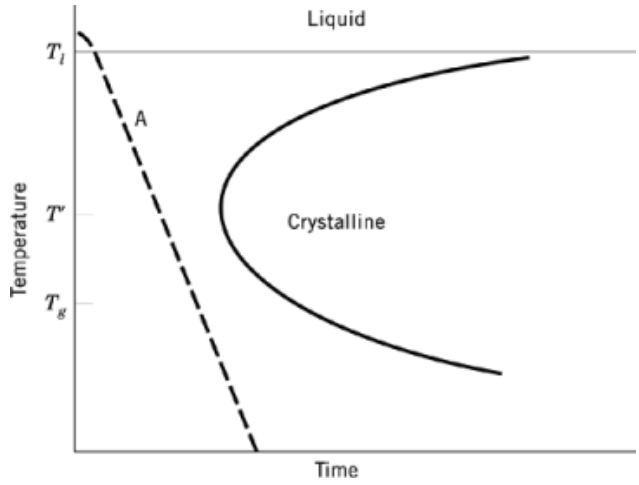

Fig. 2. Time–temperature–transformation (TTT) diagram where A represents the cooling curve necessary to bypass crystallization. The C-shaped curve separates the amorphous solid region from the crystalline solid region. Terms are defined in text.

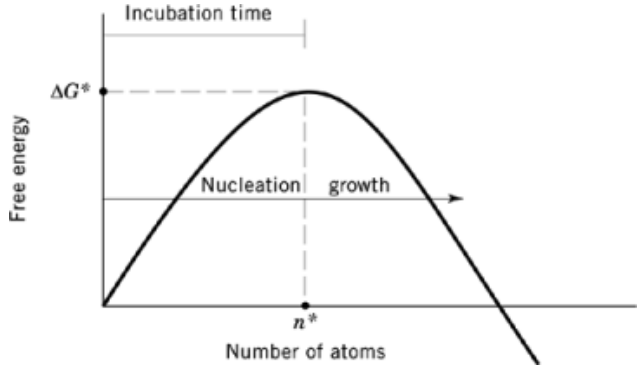

Fig. 3. Curve illustrating the activation energy (barrier) to nucleate a crystalline phase. The critical number of atoms needed to surmount the activation barrier of energy ΔG^* is n^* and takes time equal to the incubation time. One atom beyond n^* and the crystallite is in the growth regime.

alloys having such low T_{rg} into amorphous states. Unexpectedly, despite the low T_{rg} for Al–Ni–Fe–Gd alloys, only low cooling rates are necessary for the glass formation. The observed good glass formability combined with a low reduced glass-transition temperature strongly suggests that the formation of metallic glass in Al–TM1–TM2–RE alloys, where TM1 and TM2 represent two different transition metals, is unique, and to some degree is similar to that in chalcogenide systems. This unique glass formability makes it possible to produce thick amorphous ribbons based on aluminum.

The good glass formability of Al-based glasses must ultimately be related to the atomic interactions and the structure of the amorphous state. Neutron and x-ray scattering have been applied to study the atomic structure of amorphous $Al_{90}Fe_xCe_{1-x}$ (25, 26). In these amorphous alloys, the distance of an Fe–Al pair is 0.02 nm shorter than the sum of the atomic radii of Al and Fe atoms. Further structural analysis of these data reveals that Fe atoms are surrounded by approximately 10 Al atoms (0.3 nm), and of these, six are in close contact with Fe. Also, the rare-earth atoms in Al–Fe–Ce metallic glasses form a dilute dense random

packing substructure, and repel each other, whereas the substructure of Fe atoms and the surrounding Al atoms are substantially different from the random packing. The strong Al–Fe interaction suggested from structural studies is consistent with the large negative volume additivity of the Al–Fe alloys in the liquid or solid state (27). Furthermore, an Al melt actually contracts with a small addition of Fe, and more remarkably the shear viscosity of molten Al is sharply increased by dissolution of small amounts of Fe (28). Based on these analyses, the unusual glass formability in Al–TM–RE may be explained by an increase in the shear viscosity of the molten alloy through Al–TM interactions (29) resulting in a high resistance to nucleation and crystallization. The amorphous arrangement of Al–TM clusters is further stabilized by the randomly distributed rare-earth atoms. This behavior occurs through the entire supercooling process to temperatures lower than glass temperature T_g assuring the glass formation.

Among metallic glasses, only a few alloys have high resistance to nucleation and crystallization during the quenching process; examples are Pd–Cu–Si and Pd–Ni–P alloys which can be water quenched into amorphous rods of 2-mm diameter (30). In this case, the critical cooling rate for amorphous phase formation is reduced to a few hundred degrees per second. It has been demonstrated that upon the elimination of heterogeneous nucleation sites, critical cooling rates as low as a few degrees per second are sufficient to allow the formation of an amorphous phase in $Pd_{40}Ni_{20}P_{20}$ alloy (31). Adding a second transition metal to Al-based glasses greatly enhanced the glass-forming ability and submillimeter thick Al–Ni–Co–Y (32) and Al–Ni–Fe–Gd (29) amorphous ribbons can be produced at rather low quenching rates. The search for metallic glasses having superb glass-forming ability and high resistance to nucleation and growth was quickly extended to Mg-based ternary alloys containing rare earths where amorphous rods of $Mg_{65}Cu_{25}Y_{10}$ having a diameter of 4 mm could be produced (33). Replacing part of the transition metal in La–Al–TM (34) and Nd–Al–TM (35) alloys by one or more other transition-metal elements drastically enhances the glass formability (36). Using a high pressure die-casting method, the maximum diameter of an amorphous alloy rod in $La_{55}Al_{25}Ni_{10}Cu_5Co_5$ could be increased to 9 mm, and the resulting critical cooling rate Fig. 2 for glass formation is estimated to be less than 100 K/s. More recently, the formation of amorphous Zr–Ti–Cu–Ni–Be alloy rod having a diameter of up to 14 mm was produced using a water quenching method at a critical cooling rate less than 10 K/s (4). The diversity of atomic species and the large variation in atomic size plays an important role in the amorphous phase formation in these alloys. These results demonstrate that a wide variety of glasses can be produced in bulk form that can then be cast and later machined into useful components, such as small gears (37). The ability to produce bulk metallic glasses gives added confidence that these materials may find structural uses.

3. Processing

Traditionally, production of metallic glasses requires rapid heat removal from the material (Fig. 2) which normally involves a combination of a cooling process that has a high heat-transfer coefficient at the interface of the liquid and quenching medium, and a thin cross section in at least one-dimension. Besides rapid cooling, a variety of techniques are available to produce metallic glasses. Processes not dependent on rapid solidification include plastic deformation (38), mechanical alloying (7, 8), and diffusional transformations (10).

Splat quenching or gun techniques involve rapid solidification through atomizing molten metal by blowing it out a tube. The resulting liquid vapor is quenched by impingement upon a metal substrate having a high thermal coefficient. Development of this simple technique opened the window to a whole new world of novel alloys, ie, metallic glasses and other metastable crystalline and quasicrystalline alloys. Because of the undesireable characteristics of the small size of the resulting material and its irregular thickness, other techniques followed. The piston and anvil (39) and twin pistons (Fig. 4**a**) are two of these. Splat quenching results in an irregular foil of variable thickness. The approach is suitable for research but not for commercial production.

Melt-spinning can produce large quantities of very uniform ribbons, filaments, or tapes. The product is made in continuous form. Most simply, the metal is melted by induction in a chamber (Fig. 4**b**) and then expelled

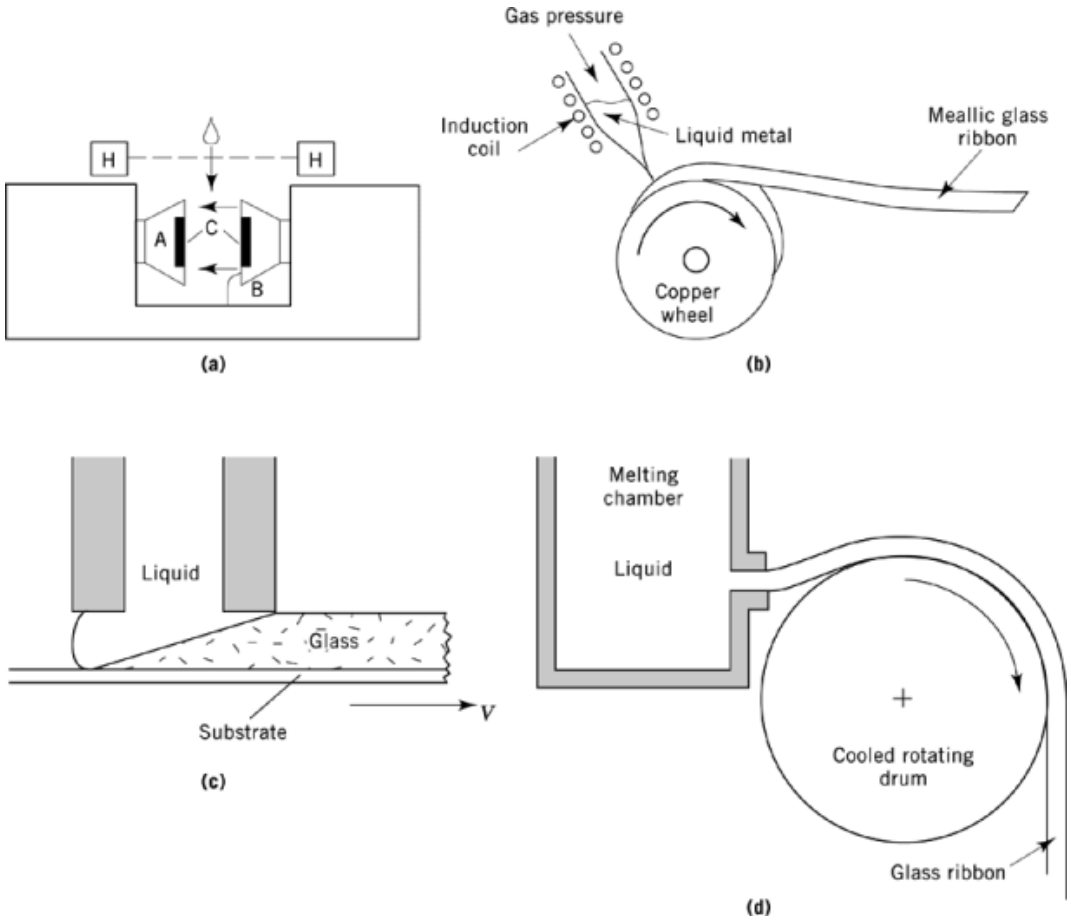

Fig. 4. Schematic diagrams of (**a**) piston-anvil quenching (39), where A is the fixed anvil; B, the fast-moving piston; C, copper disks; and H, photo cells; (**b**) melt-spinning apparatus; (**c**) planar flow casting; and (**d**) melt drag process.

onto a rotating wheel of high thermal conductivity, eg, copper. The rapidly formed ribbon is then collected in a catch chamber. The quench rate (10^5–10^8 K/s) determines the thickness and width of the final product which usually can be from 20–300 μm thick and from a few to hundreds of mm wide. For example, increasing wheel speed from 27 to 47 m/s decreases the ribbon thickness from 37 to 22 μm for an $Fe_{40}Ni_{40}B_{20}$ alloy (40). This technique has the drawback of short contact times between the molten alloy jet and the wheel. This in turn limits the available cooling rate. A more recent development is centrifuge melt spinning (41). Here the alloy is induction melted and centrifugal force impinges the melt onto the inner surface of a copper rim. This technique can produce cooling rates of 10^8 K/s (42) and the ribbon has a more uniform thickness than using conventional melt spinning.

The production of wide (>5 mm) ribbons requires a technique whereby a rectangular melt is forced through a slotted nozzle very close (0.5 mm) to the cooling substrate (Fig. 4**c**) rotating at high speed. This technique is called planar flow casting (43) and is responsible for large-scale production of continuous metallic glass tapes. Ribbons as wide as 300 mm have been produced (44) using this technology.

The melt drag process drags molten metal from an orifice onto a cooled drum (Fig. 4**d**) (45). Ribbons in excess of 20 cm can be produced having thicknesses from 25 to 1000 μm (46). Gravity is used to force the molten

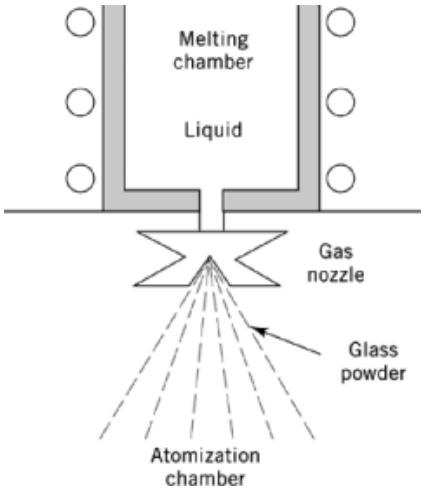

Fig. 5. Schematic diagram of the gas atomization process.

liquid from the orifice so that it touches the rotating drum. The partially solidified alloy is then dragged onto the drum forming wire or ribbons.

Lasers (qv) can be used to obtain very fast quench rates up to 10^8 K/s. A thin layer is melted on the surface of a material. The high energy density generated can melt small areas rapidly where the resulting amorphous layer is up to 400 μm in $Pd_{91.7}Cu_{4.2}Si_{5.1}$ (47, 48). Techniques of altering the surface chemistry by feeding in elemental or alloy powders on the surface prior to melting also exist using this approach (49). Electron-beam surface melting is a similar technology (see Surface and interface analysis).

Metallic glass powders can be made in various sizes through atomization and comminution processes. Atomization can be accomplished by a variety of techniques (50–54) including gas (Fig. 5), gas–liquid (55, 56), and ultrasonic gas atomization (57, 58). Cooling speeds vary from 10^5–10^9 K/s depending on the approach used and the diameter of the powder produced (59, 60). After the powder is sized, it must then be consolidated by other techniques such as warm pressing or extrusion. Using these techniques, crystallization and embrittlement can be difficult to avoid. Dynamic or quick processing has been applied to consolidate the amorphous powders (61, 62). Atomization of $Al_{85}Ni_{10}Mm_5$, where Mm is misch metal (see Cerium and cerium compounds), into powders of 13 μm average diameter has been successfully consolidated, and warm (453 K) material has been extruded with a cross-sectional reduction area of 40% (63). Samples $2 \times 2 \times 4$ mm^3 were compressively tested from the compact having strengths of 1060 MPa (147,700 psi). This was the first demonstration that bulk amorphous materials could be produced by powder metallurgy techniques.

Ion implantation (qv) has a large (10^{14} K/s) effective quench rate (64). This surface treatment technique allows a wide variety of atomic species to be introduced into the surface. Sputtering and evaporation methods are other very slow approaches to making amorphous films, atom by atom. The processes involve deposition of a vapor onto a cold substrate. The buildup rate (20 μm/h) is also sensitive to deposition conditions, including the presence of impurity atoms which can facilitate the formation of an amorphous structure. An approach used for metal–metalloid amorphous alloys is chemical deposition and electrodeposition.

The first solid-state amorphization reaction observed (65) was the loading of a binary metallic Zr–Rh metastable crystalline phase with hydrogen. The result of raising the free energy of this metastable phase through hydrogen loading is decomposition of the phase to form an amorphous hydride. The metastable hydride is more stable than the hydrogen-loaded crystalline phase under the conditions of the experiment. This amorphous phase is only stable in a limited high temperature range. More work on solid-state amorphization

(10) led to the conclusion that transformation to an amorphous phase is possible in any binary metallic system demonstrating anomalous diffusion where one type of atom has a much higher mobility than the other within the working temperature range. By producing specially made binary structures having very thin elemental layers, which can then be annealed to provide activation energy for diffusion, such systems can be used to form bulk amorphous samples of almost any size as long as the elemental layers are thin enough for thorough interdiffusion (66).

Not long after the solid-state work, it was noticed that very thin-layered microstructures were obtainable by mechanical milling elemental powders, a process which could be directly applicable to solid-state amorphization (7, 8). More recently, investigations have been carried out on the formation of amorphous phase through solid-state reactions, typically by the use of mechanical alloying and interdiffusion between thin films (qv). Because these solid-state transformations do not rely on high heat-transfer rates, there is the possibility of forming bulk amorphous material having much larger dimensions through powder metallurgy than through rapid solidification techniques. Mechanical alloying can be performed by any of several methods, but the most common is ball milling. Using this method, alloys are formed by placing the constituent elemental powders into a hardened metal jar with a number of hard metal balls, then sealing the jar, usually under some inert atmosphere to prevent powder oxidation, and placing the jar into a machine that shakes it for a long period of time, until the elemental powders are so intimately cold-welded and interdeformed that they transform into powdered alloy. In the case of easily amorphizable alloy systems, the powder product is often seen to be the amorphous phase. Never during the process does any material melt, therefore eliminating all consideration of rapid solidification phenomena. At short milling times, when the elemental powders have not yet interdeformed to the extent that they have lost their individual identities, a fine structure of highly deformed cold-welded elemental layers is observed, analogous to kneading balls of different colored modeling clay together. It has been shown that amorphous powders can be formed simply by mechanically milling, and thereby mechanically alloying, the elemental powders of an appropriate binary metallic system such as Ni–Zr (67). Particularly useful is the fact that the milling process itself produces enough localized thermal energy to drive the interdiffusion and lead to amorphization. The structure of the amorphous phase formed in this way is essentially the same as that produced through rapid-quenching (67). Application of this technique to $Al_{80}Ni_8Fe_4Gd_8$ (68) where the elements are mixed and ball milled up to 80 hours is shown in Figure 6 where x-ray diffraction traces as a function of milling time illustrates the amorphizing of this alloy.

4. Crystallization

Metallic glasses are metastable. A combination of thermal energy and time leads to crystallization. At room temperature, this may require a very long time but at moderate temperatures of 373 K or more (depending on the alloy) devitrification can occur in minutes. Usually the crystallization temperature is given as the temperature at which crystallization begins as the alloy is heated at a constant rate. Figure 7 is a differential scanning calorimeter (dsc) trace for an $Al_{85}Ni_5Fe_2Gd_8$ glass. T_x, the crystallization temperature, is defined as the onset temperature or the peak temperature of the first exotherm in the dsc scan. In this case crystallization begins at 543 K. Crystallization leads to an increase in density of about 1%. In general, T_x is somewhere between 0.4 and 0.65 T_m where T_m is the melting temperature, which for specific alloys is 400 K for Mg-based glasses and 1200 K for refractory amorphous material. The commercially important ferromagnetic iron-based glasses have T_x values of about 700 K (69).

Crystallization, by definition, implies that the initial structure be a glass, followed by the nucleation and growth of a crystalline phase, be it the equilibrium one or a metastable phase. The process is a first-order transformation and involves atomic diffusion. Types of crystallization reactions that occur include polymorphous crystallization, which is a composition invariant transformation such as that in Fe–B (70), and eutectic crystallization, T_e, in FeNiPB glass, where fine lamellae of iron–nickel austenite and metastable $(FeNi)_3PB$

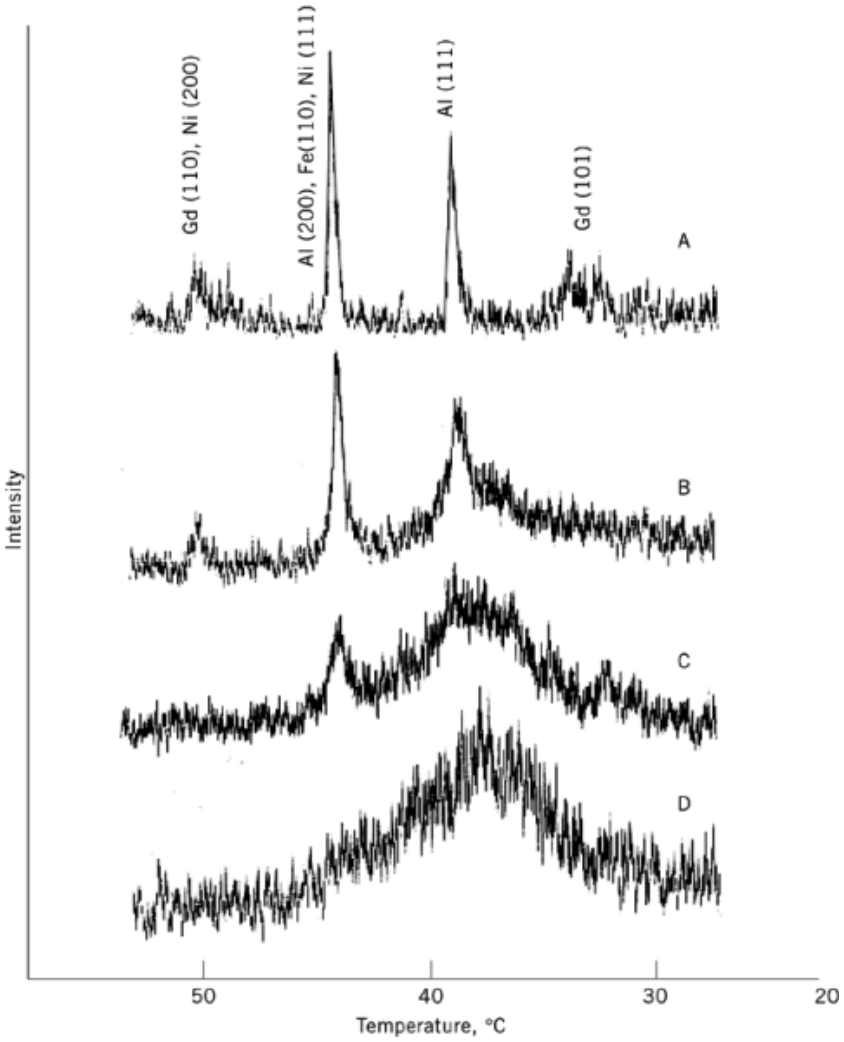

Fig. 6. X-ray diffraction traces vs ball milling (mechanical alloying) for $Al_{85}Ni_5Fe_2Gd_8$ at A, 2 h; B, 5 h; C, 20 h; and D, 80 h. After 80 hours of milling the original elemental powders are alloyed into a metallic glass (29).

phases grow cooperatively. In the primary crystallization reaction, the initial crystals formed have an overall composition different from the bulk glass (Fig. 8). The kinetics are then dependent on the rate of diffusion in the remaining glassy matrix. A more complicated mechanism is for the glassy metal to separate first into two distinct glassy phases followed by crystallization separately in each of these phases, eg, the $Zr_{36}Ti_{24}B_{40}$ system (71).

An area of some concern is whether metallic glasses are indeed amorphous (72). Amorphous materials are generally characterized by a broad diffuse x-ray or electron diffraction pattern. However, it has been a subject of intensive debate whether a material exhibiting a broad diffuse x-ray diffraction pattern has a truly amorphous structure or whether it consists of randomly oriented microcrystallites or microquasicrystallites. Thus techniques other than diffraction experiments are necessary to distinguish between the two. High resolution electron microscopy (hrem) and differential scanning calorimetry can provide direct and indirect observations

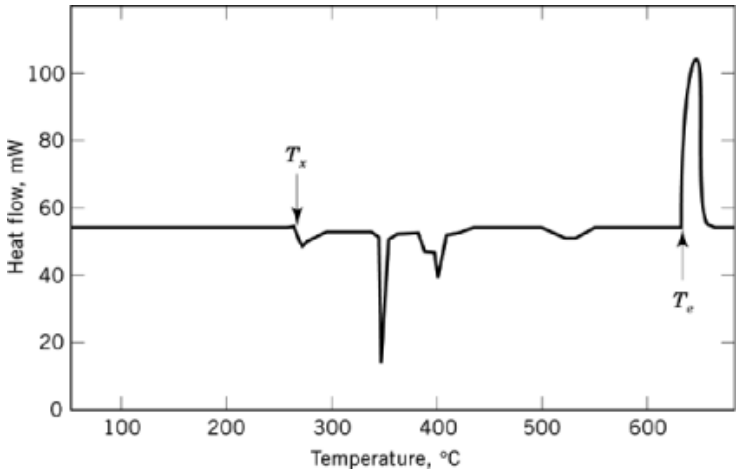

Fig. 7. Dsc scan for glassy $Al_{85}Ni_5Fe_2Gd_8$ alloy where T_x is the crystallization temperature and T_e the eutectic temperature.

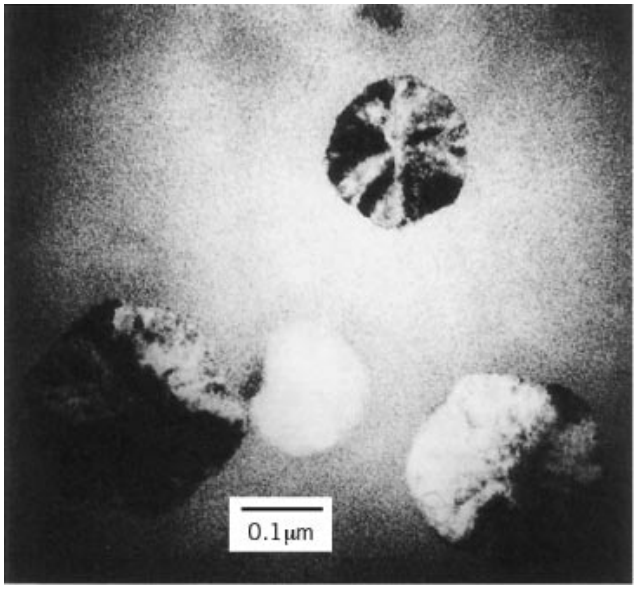

Fig. 8. Electron micrograph showing crystallization of icosahedral phase from glassy Pd–U–Si alloy.

of the structural nature of metallic glasses (see Microscopy). Modern medium voltage high resolution electron microscopy having a resolution <0.2 nm enables identification of microcrystallinity in a sample. Using calorimetric techniques to study the isothermal crystallization kinetics allows a differentiation to be made between amorphous and microcrystalline structures (73). Figure 9 shows amorphous aluminum glass and microcrystalline glass (74). The $Al_{90}Fe_5Gd_5$ samples observed in hrem do not reveal any crystalline structure in the sample (Fig. 9**a**), and the Fourier transform of the hrem image shows structureless features, providing direct evidence that the glass is truly amorphous. Annealed samples illustrate crystallization in the glass (Fig. 9**b**).

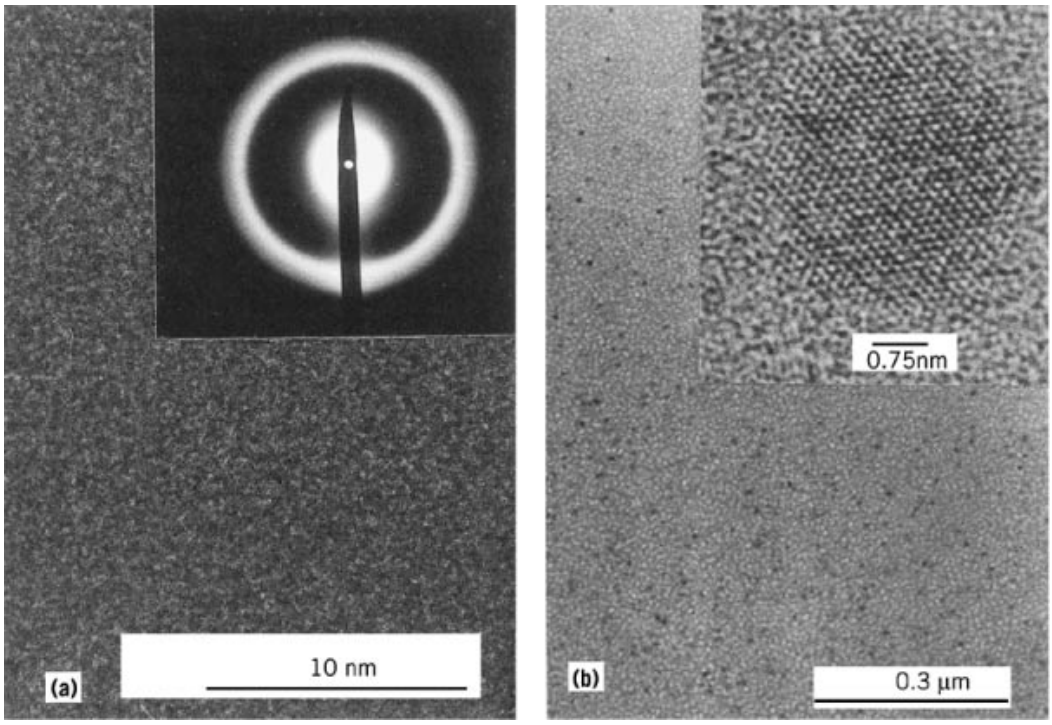

Fig. 9. (**a**) A high resolution electron micrograph of amorphous $Al_{90}Fe_5Gd_5$ alloy and its Fourier transform (inset). (**b**) Conventional electron micrograph of same alloy after annealing at 447 K for 150 minutes. The small particles are crystallites and can be imaged with high resolution electron microscopy (inset) that clearly shows the periodic nature of the crystallites which are aluminum imaged in a 110 direction.

The periodic structure is a structural image of an aluminum crystal embedded in a glassy matrix. X-rays would not differentiate crystallites this small.

To confirm that the matrix is amorphous following primary solidification, isothermal dsc experiments can be performed. The character of the isothermal transformation kinetics makes it possible to distinguish a microcrystalline structure from an amorphous structure assuming that the rate of heat released, dH/dt, in an exothermic transformation is proportional to the transformation rate, dx/dt, where H is the enthalpy and $x(t)$ is the transformed volume fraction at time t. If microcrystals do exist in a grain growth process, the isothermal calorimetric signal dH/dt is proportional to $1/r^{m+2}$, where r is the average grain size and m is a positive exponent (73). The heat-release rate decreases monotonically with time, which is the case in a sputtered Al–Mn film (73).

In an amorphous material, the alloy, when heated to a constant isothermal temperature and maintained there, shows a dsc trace as in Figure 10 (74). This trace is not a characteristic of microcrystalline growth, but rather can be well described by an isothermal nucleation and growth process based on the Johnson-Mehl-Avrami (JMA) transformation theory (75). The transformed volume fraction at time t can be written as

$$x = 1 - \exp\{-[K(t-\tau)]^n\}, \quad t > \tau$$

where $K = K_o \exp(-E_x/\mathrm{RT})$ is the reaction rate constant and E_x is the activation energy in the crystallization process, which incorporates the activation energy for both nucleation and growth of the new phases. E_x generally

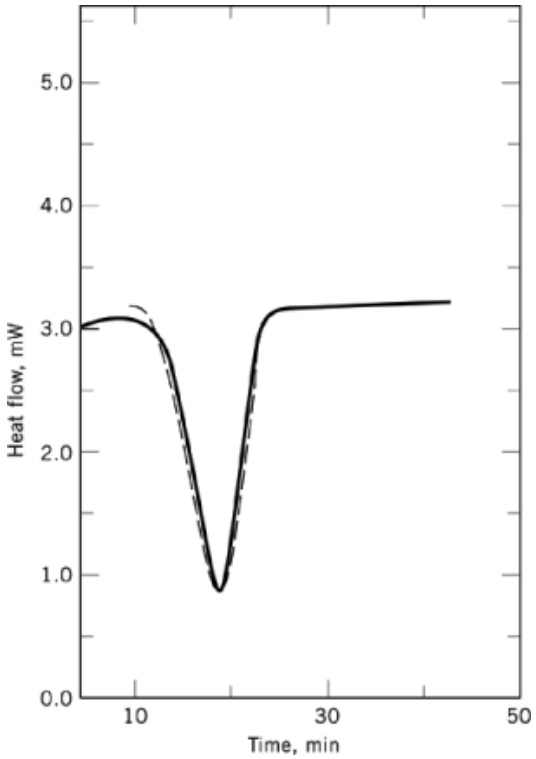

Fig. 10. An isothermal dsc trace of $Al_{90}Fe_5Gd_5$ sample at 605 K. The solid line — is experimentally determined and the dashed line (– – –) is a computer simulation according to the Johnson-Mehl-Avrami equation. The degree of overlap demonstrates that the sample was truly amorphous.

has a value between 40 and 400 kJ/mol (10 and 100 kcal/mol) (69). T is the absolute temperature, R is the gas constant, and n, the Avrami exponent, is >0 and varies between 1.5 to 4.0 (75).

Crystallization need not always be deleterious to properties such as strength. In Al-based glasses, partially crystallized material actually increased the fracture strength by 30%. A wholly amorphous $Al_{90}Fe_5Gd_5$ material obtained by melt-spinning and then annealed at 445 K for 20 minutes resulted in the nucleation and growth of nanocrystals (Fig. 9**b**) (76). These 5-nm precipitates are face-centered cubic and aluminum rich. Because of the very high ($10^{23}/m^3$) density and uniform distribution, the efficacy of the nanocrystalline amorphous matrix material in preventing the onset of fracture is high in this system.

5. Mechanical Properties

Of the various physical properties, it is the mechanical properties that make metallic glasses so unique when compared to their crystalline counterparts. A metallic glass obtains its mechanical strength in quite a different way from crystalline alloys. The disordered atomic structure increases the resistance to flow in metallic glasses so that these materials approach their theoretical strength. Strengths of $E/50$ where E is Young's modulus, are common (Table 2). An attractive feature is that metallic glasses are equally strong in all directions because of the random order of their atomic structure.

Table 2. Mechanical Properties of Metallic Glasses[a]

Alloy	Fracture strength, σ, GPa[b]	Density, ρ, mg/m^3	Specific strength, σ/ρ	Young's modulus, E, GPa[b]
$Al_{85}Ni_6Fe_3Gd_6$	1.3	3.51	0.37	72.7
$Fe_{80}B_{20}$	3.6	7.4	0.49	170
$Ti_{50}Be_{40}Zr_{10}$	2.3	4.1	0.56	105
$Cu_{50}Zr_{50}$	1.8	7.3	0.25	85

[a]Refs. 29 and 77.
[b]To convert GPa to psi, multiply by 145,000.

The ductility of glassy metals varies according to the kind of stress applied. For example, glasses are ductile when they are bent (flexible) or rolled in compression, but have little overall ductility in tension. Owing to the large intrinsic ductility, metallic glasses can be plastically deformed into useful shapes at no loss of mechanical strength. Wire drawing from $Fe_{29}Ni_{49}P_{14}B_6Si_2$ ribbons is an excellent example of this capability (78). The moduli of metallic glasses is generally less than crystalline forms of the same material. This is in part because of the atomic bonding in the metallic glass which does not have the overall symmetry of the crystalline metal. Upon supplying thermal energy, the moduli increase in association with structural relaxation. Typical ranges of elastic moduli ratios are 1.2–1.4 for crystalline to amorphous (79). Poisson's ratios are higher for metallic glasses: ~ 0.4 compared to crystalline metal values of about 0.33.

Plastic deformation in crystalline metals is accomplished by dislocation motion on specific atomic planes of atoms. Because of the random packing of atoms in amorphous metals, this mechanism is not available, and plastic flow occurs by homogeneous and inhomogeneous flow (80). The former, in which the metal glass deforms uniformly, is prevalent when stresses are less than 1/50 of the shear modulus. This occurs in creep situations. The microscopic mechanisms for homogeneous flow are based on models of free volume, microscopic shear transformation, structural relaxation, configurational entropy, and isoconfigurational flow (80). Each of these mechanisms has a temperature range where it is applicable. At temperatures between T_g and $T_g - 20$ the free volume and configurational entropy models are employed. The free volume model accounts for the temperature dependence of flow by incorporating the changes in free volume. The alteration of atomic configuration and size of flow areas are examined by the configurational entropy. At temperatures lower than $T_g - 20$, models based on structural relaxation take on increased importance. Almost by definition, the structure of the metal glass is not the equilibrium one. At temperatures below T_g, the atomic flow resulting from stress can result in increased flow resistance which may result from an increase in structural order.

Inhomogeneous flow, which occurs at higher stresses, is $>1/50$ of the shear modulus (80), and its resulting strain is in the shear band. The formation of these shear bands, which are regions of highly localized deformation, are randomly spaced. Sometimes only a single band forms prior to fracture. Strains within the shear bands are as high as 10 and the bands are very narrow (<5 nm). In tension, only one band may form, but in more complex processes such as bending, rolling, or extrusion, multiple shear bands result with many orientations (Fig. 11). The internal structure of a single shear band, examined using high resolution electron microscopy (81), revealed nanocrystals in an $Al_{90}Fe_5Gd_5$ amorphous ribbon. The ribbon was bent through 180 degrees generating a high density of slip bands that were measured to be 5 nm in width. The deformation process resulted in aluminum-rich nanocrystals forming, all within slip band and surrounded by the glassy matrix. Whereas the fracture strength of a metallic glass may nearly equal its yield strength in tension, thus labeling the material brittle, compound deformation modes may enable the ductility of a metallic glass to be as high as 100% (bending).

The fracture of metallic glasses occurs by the formation of shear bands having a 45° orientation relative to the tensile axis. Typical veining on the fracture surface is a characteristic of almost all metallic glasses (82). The smooth curvature of the veins results from necking of the material (Fig. 12) and involves considerable

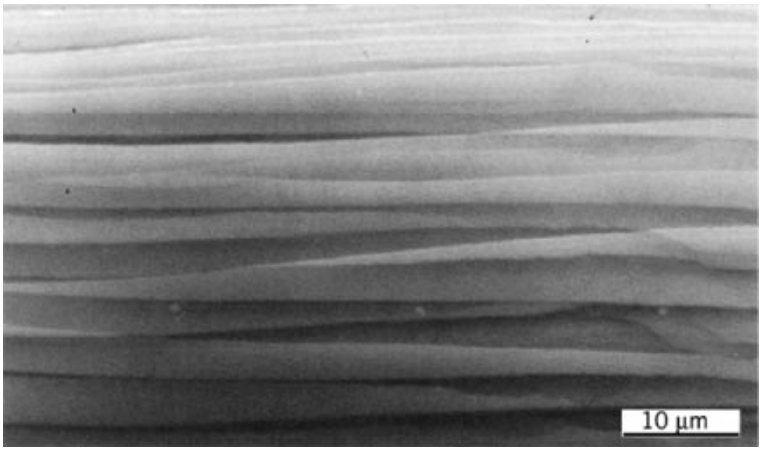

Fig. 11. Scanning electron micrograph showing the intersection of primary shear bands with the glassy ribbon surface produced by simple bending.

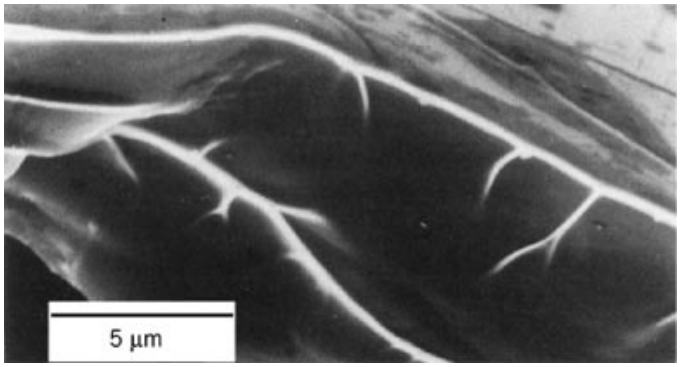

Fig. 12. Typical fracture surface of metallic glass.

viscous flow which has been described as the result of shear displacements along the shear band implying that the glassy metal is tough because the crack tip is dull (82). However, it is along the shear band that microcracks nucleate and propagate until impinging upon other cracks. The result of this intersection is that necking begins leading to the veining pattern.

The deleterious embrittlement of a glassy metal during annealing is also accompanied by a change in fracture mode. Almost all metallic glasses containing Fe, Co, and Al show this behavior. Figure 13 illustrates the transition to brittle fracture. When an Al–Fe–Gd glass is tested in tension, the ribbons fail by fracture along shear bands oriented at 45° to the tensile axis. The fracture surface has the typical veining pattern. After annealing at 543 K for 20 minutes, the fracture mode begins changing to a brittle fracture at 90° to the tensile axis, and a much different fracture surface is seen.

Fracture toughness experiments have been accomplished using tear tests to determine the critical stress intensity factor, K_{IIIC} (83). Iron-based glasses have a lower fracture toughness than crystalline materials such as AISI 4340 and maraging steels (84) (see Steel). This is a result of the substantially increased yield strengths of the metallic glasses which in turn is a result of the lack of plasticity in glassy materials.

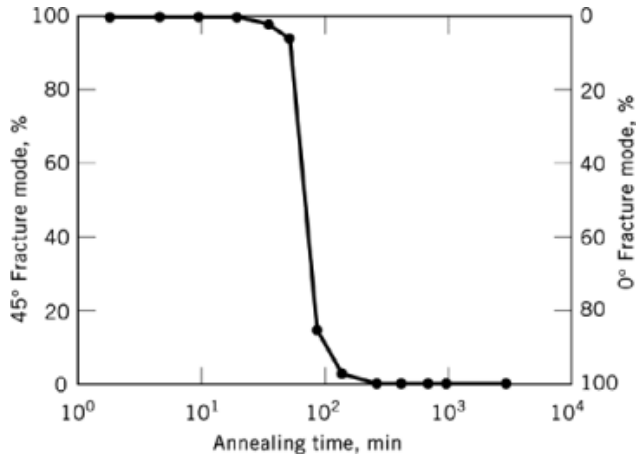

Fig. 13. Transition between ductile fracture and brittle fracture when $Al_{90}Fe_5Gd_5$ metallic glass is annealed at 170°C.

At low applied stress levels crystalline alloys display fatigue properties superior to metallic glasses. At large loads approaching the fracture strength, metallic glasses can survive many more cycles than comparable strength crystalline alloys. This is because the metallic glass deforms elastically up to the high stress levels, whereas crystalline alloys generate localized regions of plastic deformation which lead to nucleation of fatigue cracks. In a $Pd_{80}Si_{20}$ alloy the fatigue crack propagation rate follows the same dependence as crystalline alloys (85):

$$da/dN = A\Delta K^m$$

where a is the crack length, N the number of cycles, ΔK the cyclic stress intensity, and A and m the material constants.

6. Properties

6.1. Chemical

Along with magnetic and mechanical behavior, high corrosion resistance is one of the most desirable properties of metallic glasses. The lack of crystalline defects, including grain boundaries and dislocations, helps to ensure that metallic glasses have attractive electrochemical properties. Coupled with this is the induced passivity owing to elements such as Cr and Al, and rapid repassivation following damage to the surface film. Corrosion rates can be increased by several orders of magnitude by introducing second phases by further processing steps including annealing or mechanical working, eg, warm extrusion, which could have a chemical potential difference. When elements such as Cr are added to the alloy, these enrich the surface film through the formation of complex hydroxides, eg, $CrO_x(OH)_{3-2x}{\cdot}nH_2$ (86). The amount and type of metalloid also influences the corrosion resistance of the passivating film. Adding P and C together in an $Fe_{70}Cr_{10}P_{13}C_7$ dramatically increases the concentration of Cr that appears on the surface film (87). In most instances the general overall corrosion resistance is determined by the presence of a passivation element rather than the amorphous nature of the alloy (88).

Table 3. Magnetic Properties[a]

Alloy	Coercive field, H_c, A/m[b]	Curie temp, θ_c, °C
$Fe_{80}B_{20}$[c]	3.1	374
$Fe_{80}P_{16}B_1C_3$[d]	4.0	292
$Fe_3Co_{72}P_{16}B_6Al_3$	1.2	260
$Fe_{96.8}Si_{3.2}$[e]	20–40	730

[a] Ref. 93.
[b] To convert A/m to oersted, multiply by 0.0126.
[c] Metglas 2605.
[d] Metglas 2615.
[e] Material is crystalline.

6.2. Magnetic

More experimental research and developmental work has been done on magnetic effects in metallic glasses than any other property (89). This is, of course, because of the focus of the technological and commercial importance (90, 91). The first important glassy ferromagnet was $Fe_{83}P_{10}C_7$ (92). Alloy compositions that produce useful magnetic amorphous structures stable at room temperatures contain large fractions of transition-metal or rare-earth elements. Combinations of transition metals (primarily Fe, Ni, and Co), between 75 and 84 atom % and metalloid or glass-forming elements including C, P, B, Si, and Ge, around 20%, produce glasses strongly magnetic at room temperature. Adding a second transition metal allows ribbons of greater thicknesses to be produced. This benefit leads to multiple elements being employed. Table 3 (93) compares some properties of amorphous alloys with a crystalline-oriented FeSi transformer steel.

The Curie temperature for several magnetic glasses has been experimentally determined (89, 94). This temperature represents the point where thermal agitation of the mutual interactive forces of atomic dipoles, which tend to align neighboring dipoles to one another, are perturbed. The net average moment is zero at the Curie temperature. Metallic glasses have a low Curie temperature relative to crystalline alloys. The results show that substituting Ni for Fe raises the Curie temperature in glasses such as $(Fe_xNi_{1-x})_{80}B_{20}$·FeCo alloys which have a broad maximum in Curie temperature near a Fe/Co ratio of 1. As Fe content is further increased, the Curie temperature is decreased which may reflect the atomic packing. Alloying the metallic glasses with metalloid and additional transition-metal additions has predictable effects. For example, when transition metals Cr, Mo, or V are substituted for Fe, the Curie temperature is lowered precipitously. The addition of P has a tendency to effect lower values of Curie temperature than the addition of B. Alloys having two or more transition metals have a less sharply defined Curie temperature than those having only one. The reason for this may be chemical inhomogeneity and phase separation.

For binary iron-based amorphous alloys, the saturation magnetization, ie, maximum magnetic moment per unit volume, is linear with metalloid content at low temperatures (95). As temperature is raised, the saturation magnetization increases, reaches a peak value, then drops suddenly owing to the Curie temperature relationship with increasing metalloid content. Values for saturation magnetization have been collected for a large number of ferromagnetic amorphous alloys. Fe_xB_{100-x} alloys have shown the largest magnetization values (96). Saturation magnetization values for metallic glasses are generally lower than for crystalline alloys because of the presence of metalloid atoms which contribute to a higher volume of atoms without magnetic moments. One of the primary parameters for soft magnetic materials is the static coercivity, H_c. For metallic glasses this value is very low (Table 3).

Amorphous alloys are not perfectly homogeneous because these materials do not show isotropic magnetic properties. Real glasses have varying amounts of magnetic anisotropy. The reasons are plentiful and include not only nonhomogeneous segregation of alloying elements but also internal stresses, both chemical and mechanical, resulting from cooling differences, and final processing of the material.

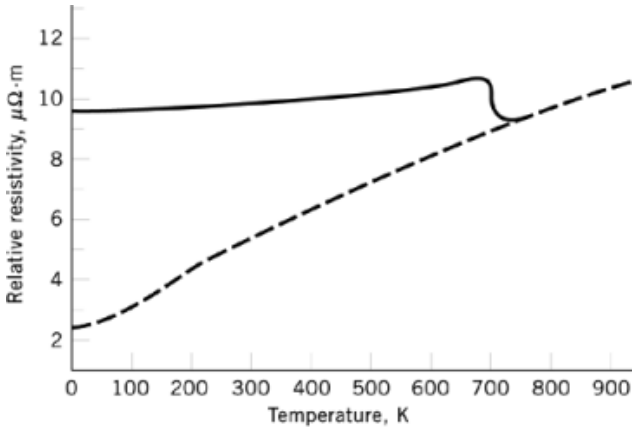

Fig. 14. Relative resistivity of FePC as (—) a glass, and (– – –) in crystalline form.

6.3. Electrical

Unlike their crystalline counterparts, amorphous metals generally have high electrical resistivity not only at room temperature, but also, because of a very small temperature coefficient, near absolute zero. This can be understood by the atomic nature of the glass; that is, the randomness of the structure which efficiently scatters electrons. Figure 14 illustrates the difference between amorphous and crystalline FePC (97). The resistivity of the glass has little temperature dependence until it crystallizes at 675 K. Certain metallic glasses, eg, $La_{80}Au_{20}$ (98), do show superconductivity. The critical temperature is as high as 8.7 K. Metallic glass superconductors are also relatively insensitive to composition (99) and have very short electron mean-free paths.

7. Uses

The magnetic properties of glassy metals provide the only commercial use in bulk quantities, although brazing foils provide another niche for metallic glasses. Metallic glasses have yet to find their way into commercial products in structural applications in spite of the great strength of some glasses. This is related to their shearing instability and size limitations of the glassy product which requires a fabrication step to obtain bulk material.

7.1. Magnetic Applications

Metallic glasses are utilized in electric transformers and this provides a significant commercial success for these materials. Alloys such as MetGlas 2605 SC, $Fe_{81}B_{13.5}Si_{3.5}C_2$, are prepared in sheets having superior soft magnetic properties. These alloys can be magnetized and demagnetized with low remnant magnetizations. This is manifested in a much narrower hysteresis loop than found in an Fe—Si alloy which is the prime competing crystalline alloy to metallic glasses. The large magnetization response coupled with low magnetic losses and low excitation power make amorphous magnetic alloys attractive in applications such as transformers and inductors (100). In the United States and Japan amorphous metal-cored transformers are replacing distribution transformers where the cores are based on Fe—Si. The amorphous metals provide much lower energy losses under alternating current excitation. Amorphous metals can be also woven into sheets for magnetic shielding applications.

The combination of properties found in metallic glasses make them good candidates for recording heads where magnetic properties combined with wear resistance and mechanical hardness are attractive. Metallic glasses have often been considered for mechanical applications because of their combination of high strength and toughness. Upon discovery of aluminum glasses, these materials can also be lightweight. Suggestions for applications include rivets, razor blades, and tire cords. As of this writing, none have come to realization (101). The progress made in casting large ingots of metallic glass (4) opens up the possibility of casting and machining small components such as gears.

BIBLIOGRAPHY

"Glassy Metals" in *ECT* 3rd ed., Vol. 11, pp. 893–910, by T. Egami, Max-Planck Institut für Metallforschung.

Cited Publications

1. P. Duwez, R. H. Willens, and W. Klement, Jr., *J. Appl. Phys.* **31**, 1136 (1960).
2. R. W. Cahn, in R. W. Cahn and P. Haasen, eds., *Physical Metallurgy*, 3rd ed., Elsevier Science Publishers, Amsterdam, 1983, p. 1779.
3. P. Duwez, in P. Duwez, *Concise Encyclopedia of Solid State Physics*, Addison-Wesley, Reading, Mass., 1983, p. 112.
4. A. Peker and W. L. Johnson, *Appl. Phys. Lett.* **63**, 2342 (1993).
5. Y. Kawamura, A. Inoue, and T. Masumoto, *Scripta Metall. Mater.* **29**, 25 (1993).
6. H. Jones, *J. Mater. Sci.* **19**, 1043 (1984).
7. E. Hellstern and L. Schultz, *Appl. Phys. Lett.* **48**, 124 (1986).
8. E. Hellstern and L. Schultz, *J. Appl. Phys.* **63**, 1408 (1988).
9. G. K. Wehner and G. S. Anderson, in L. I. Maissel and R. Glang, eds., *Handbook of Thin Film Technology*, McGraw-Hill, New York, 1970, 1–3.
10. R. B. Schwartz and W. L. Johnson, *Phys. Rev. Lett.* **51**, 415 (1983).
11. J. L. Finney, in F. E. Luborsky, ed., *Amorphous Metallic Alloys*, Butterworths, London, 1983, p. 42.
12. F. Spaepen, in M. B. Bever, ed., *Encyclopedia of Material Science and Engineering*, Pergamon Press, Oxford, U.K., 1986, p. 2976.
13. J. D. Bernal, *Proc. R. Soc. London A* **284**, 299 (1964).
14. P. H. Gaskell, *J. Non-Cryst. Solids* **32**, 207 (1979).
15. S. R. Elliott, *Physics of Amorphous Materials*, Longman, London, 1983, p. 311.
16. Y. He, S. J. Poon, and G. J. Shiflet, *Science* **241**, 1640 (1988).
17. G. J. Shiflet, Y. He, and S. J. Poon, *J. Appl. Phys.* **64**, 6863 (1988).
18. A. Inoue, K. Ohtera, A. P. Tsai, and T. Masumoto, *Jpn. J. Appl. Phys.* **27**, L479 (1988).
19. A. Inoue, K. Ohtera, T. Zhang, and T. Masumoto, *Jpn. J. App. Phys.* **27**, L1583 (1988).
20. M. G. Scott, in Ref. 11, p. 144.
21. H. A. Davis, *Phys. Chem. Glasses* **17**, 159 (1976).
22. H. A. Davis, in Ref. 11, p. 8.
23. F. Spaepen and D. Turnbull, *A. Rev. Phys. Chem.* **35**, 241 (1984).
24. R. Azoulay, H. Thibierge, and A. Brenac, *J. Non-Cryst. Solids* **18**, 33 (1975).
25. H. Y. Hsieh and co-workers, *J. Mater. Res.* **5**, 2807 (1990).
26. H. Y. Hsieh, T. Egami, Y. He, S. J. Poon, and G. J. Shiflet, *J. Non-Cryst. Solids* **135**, 248 (1991).
27. D. Turnbull, *Acta Metall. Mater.* **38**, 243 (1990).
28. E. Gebhardt, M. Becker, and S. Dorner, *Z. Metallk.* **44**, 510 (1953); *ibid.*, **44**, 573 (1953).
29. Y. He, G. M. Dougherty, G. J. Shiflet, and S. J. Poon, *Acta Metall. Mater.* **41**, 337 (1993).
30. H. Chen, *Acta Metall.* **22**, 1505 (1974).
31. A. J. Drehman, A. L. Greer, and D. Turnbull, *Appl. Phys. Lett.* **41**, 716 (1982).
32. A. Inoue, N. Matsumoto, and T. Masumoto, *Mater. Trans. JIM* **31**, 493 (1990).
33. A. Inoue, A. Kato, T. Zhang, S. Kim, and T. Masumoto, *Mater. Trans. JIM* **32**, 609 (1991).

34. A. Inoue, T. Zhang, and T. Masumoto, *Mater. Trans. JIM* **31**, 425 (1990).
35. Y. He, C. E. Price, S. J. Poon, and G. J. Shiflet, *Phil. Mag. Lett.* in press (1994).
36. A. Inoue, T. Nakamura, T. Sugita, T. Zhang, and T. Matsumoto, *Mater. Trans. JIM* **34**, 351 (1993).
37. L. Greer, *Nature* **366**, 303 (1993).
38. D. Kulmann-Wilsdorf and M. S. Bednar, *Scripta Metall. Mater.* **28**, 371 (1993).
39. P. Duwez, *ASM Trans. Q.* **60**, 608 (1967).
40. H. H. Liebermann, *Mater. Sci. Eng.* **43**, 203 (1980).
41. G. Rosen, J. Avissar, J. Baram, and Y. Gefen *Internat. J. Rapid Solidif.* **2**, 67 (1986).
42. J. Baram, *J. Mater. Sci.* **23**, 3656 (1988).
43. U.S. Pat. 4,142,571 (1979), M. C. Narasimhan (to Allied Chemicals).
44. W. A. Heineman, in, S. Steeb and H. Warlimont, eds., *Rapidly Quenched Metals V*, Elsevier Science Publishers, Amsterdam, 1985, p. 27.
45. D. King and W. La, *Metals* **2**, 32 (1967).
46. J. C. Hubert, F. Mollard, and B. Lux *Z. Metakkde.* **64**, 835 (1973).
47. E. M. Breinan, B. H. Kear, and C. M. Banas, *Phys. Today* **29**, 44 (1976).
48. S. M. Complex, in B. Cantor, ed., *Proceedings of the 3rd International Conference on Rapidly Quenched Metals*, Vol. **1**, The Metals Society, London, 1978, p. 147.
49. E. M. Breinan, D. Snow, C. O. Brown, and B. H. Kear, in R. Mehrabian, B. H. Kear, and M. Cohen, eds., *Rapid Solidification Processing: Principles and Technology*, Claitor's Publishing Development, Baton Rouge, La., 1978, p. 440.
50. R. J. Grandzol and J. A. Tallmadge, *Int. J. Powder Metall. Powder Technol.* **11**, 103 (1975).
51. M. R. Glicksman, R. J. Patterson, and N. E. Schockey, in Ref. 50, p. 46.
52. P. R. Holiday, A. R. Cox, and R. J. Patterson, in Ref. 50, p. 98.
53. A. R. E. Singer, A. D. Roche, and L. Day, *Powder Metall.* **23**, 81 (1980).
54. A. R. E. Singer and A. D. Roche, in E. N. Aqua and C. I. Whitman, eds., *Modern Developments in Powder Metallurgy*, Metal Powder Industries Federation, Princeton, N. J., 1977, p. 127.
55. S. A. Miller and R. J. Murphy, *Scripta Metall.* **13**, 673 (1979).
56. S. A. Miller and R. J. Murphy, in R. Mehrambian, B. H. Kear, and M. Cohen, eds., *Rapid Solidification Processing: Principles and Technologies II*, Claitor's Publishing Division, Baton Rouge, La., 1980, p. 385.
57. N. Grant, in Ref. 50, p. 230.
58. V. Anand, A. J. Kaufman, and N. J. Grant, in Ref. 57, p. 273.
59. T. Yamaguchi and K. Narita, *IEEE Trans. Magn.* **MAG-13**, 1621 (1977).
60. A. E. Berkowitz and J. L. Walter, in Ref. 57 p. 294.
61. C. F. Cline and R. W. Hopper, *Scripta Metall.* **11**, 1137 (1977).
62. C. F. Cline, J. Mahler, F. Milton, W. Kuhl, and R. Hopper, in Ref. 50, p. 380.
63. Y. Kawamura, A. Inoue, and T. Masumoto, *Scripta Metall. Matr.* **29**, 25 (1993).
64. L. Mendoza-Felis, *Phys. Rev. B* **26**, 1306 (1982).
65. X. L. Yeh, K. Samwer, and W. L. Johnson, *Appl. Phys. Lett.* **49**, 146 (1983).
66. L. Schultz, in M. von Allmen, ed., *Proc. Materl. Res. Soc. Europe Meeting on Amorph. Metals and Non-Equil. Processing*, Les Ulis, Les Editions de Physique, Strasbourg, 1984, p. 135.
67. L. Schultz, *Phil. Mag. B* **61**, 453 (1990).
68. G. M. Dougherty, G. J. Shiflet, and S. J. Poon, *Acta Metall. Mater.* **41** (1993).
69. M. G. Scott, in Ref. 12, p. 2968.
70. A. L. Greer, *Acta Metall.* **30**, 171 (1982).
71. L. Tanner and R. Ray, *Scripta Metall.* **14**, 1657 (1980).
72. G. S. Cargill, *Solid St. Phys.* **30**, 227 (1975).
73. L. C. Chen and F. Spaepen, *Nature* **336**, 366 (1988).
74. Y. He, H. Chen, G. J. Shiflet, and S. J. Poon, *Phil Mag. Lett.* **61**, 297 (1990).
75. J. W. Christian, *The Theory of Transformations in Metals and Alloys*, 2nd ed., Pergamon, New York, 1975.
76. H. S. Chen, Y. He, G. J. Shiflet, and S. J. Poon, *Scripta Metall. Mater.* **25**, 1421 (1991).
77. R. W. Cahn, *Contemp. Phys.* **21**, 43 (1980).
78. S. Takayama, *J. Mater. Sci.* **16**, 269 (1981).

79. D. Weaire, M. F. Ashby, J. Logan, and M. J. Weins, *Acta Metall.* **19**, 779 (1971).
80. F. Spaepen and A. J. Taub, in F. E. Luborsky, ed., *Amorphlus Metallic Alloys*, Butterworths, London, 1983, p. 231.
81. H. Chen, Y. He, G. J. Shiflet, and S. J. Poon, *Nature* **367**, 541 (1994).
82. H. J. Leamy, H. S. Chen, and T. J. Wang, *Metall. Trans.* **3**, 699 (1972).
83. H. Kimura and T. Masumoto, *Scripta Metall.* **9**, 211 (1975).
84. L. A. Davis, in L. A. Davis, *Metallic Glasses*, American Society for Metals, Metals Park, Ohio, 1978, p. 190.
85. T. Ogura, K. Fukushima, and T. Masumoto, *Scripta Metall.* **9**, 979 (1975).
86. K. Asami, K. Hahimoto, T. Masumoto, and S. Shimodaira, *Corrosion Sci.* **16**, 909 (1976).
87. T. Masumoto and K. Hadhimoto, *Ann. Rev. Mater. Sci.* **8**, 215 (1978).
88. K. Hashimoto, in Ref. 81, p. 471.
89. C. D. Graham, Jr. and T. Egami, *Ann. Rev. Mater. Sci.* **8**, 423 (1978).
90. F. E. Luborsky and L. A. Johnson, *J. de Physq. (Paris)* **41**, 820 (1980).
91. D. Raskin and C. H. Smith, in Ref. 81.
92. P. Duwez and S. C. H. Lin, *J. Appl. Phys.* **38**, 4096 (1967).
93. F. E. Luborsky, in R. A. Levy and T. Hasegawa, eds., *Amorphous Magnetism II*, Plenum Publishing Corp., New York, 1977.
94. F. E. Luborsky, J. D. Livingston, and G. Y. Chin, *Physical Metallurgy*, North Holland Publishers, Amsterdam, 1983, p. 1674.
95. F. E. Luborsky, *J. Magn. Mater.* **7**, 143 (1978).
96. N. S. Kazama, M. Mitera, and T. Masumoto, *Proceedings of the Third International Conference on Rapidly Quenched Metals*, The Metals Society, London, 1978, p. 164.
97. P. Duwez, *Ann. Rev. Mat. Sci.* **61**, 83 (1976).
98. T. Masumoto, K. Hashimoto, and M. Naka, in B. Cantor, ed., *Rapidly Quenched Metals III*, Vol. **2**, The Metals Society, London, 1978, p. 435.
99. M. M. Collver and R. H. Hammond, *Phys. Rev. Lett.* **30**, 92 (1972).
100. F. E. Luborsky, *Amorphous Metallic Alloys*, Butterworths, London 1983, p. 360.
101. K. Ohtera, A. Inoue, and T. Masumoto, *Mater. Sci. Eng.* **A134**, 1212 (1991).

GARY J. SHIFLET
University of Virginia

Related Articles

Magnetic materials, bulk; Magnetic materials, thin film; X-ray technology; Crystallization; Zone refining; Microscopy